Diurnal Cloud and Thermodynamic Variations in the Stratocumulus Transition Regime: A Case Study Using In Situ and Remote Sensors

MARK A. MILLER

Department of Applied Science, Brookhaven National Laboratory, Upton, New York

MICHAEL P. JENSEN AND EUGENE E. CLOTHIAUX

Department of Meteorology, The Pennsylvania State University, University Park, Pennsylvania

(Manuscript received 4 February 1997, in final form 22 October 1997)

ABSTRACT

Radiosonde, in situ, and surface-based remote sensor data from the Atlantic Stratocumulus Transition Experiment are used to study the diurnal cycle of cloud and thermodynamic structure. A cloud layer and decoupled subcloud layer separated by a stable transition layer, often observed in the vicinity of cumulus cloud base, characterizes the thermodynamic structure during the study period. The mode of cloud structure is cumulus with bases below decoupled stratus. Data are presented that support the hypothesis that diurnal variations in cumulus development are modulated by the stability in the transition layer.

The frequency of cumulus convection decreases during the afternoon, but mesoscale regions of vigorous cumulus with cloud tops overshooting the base of the trade inversion and increased surface drizzle rates are present during the late afternoon and early evening, when the transition layer is the most stable. It is postulated that mesoscale organization may be required to accumulate enough water vapor in the subcloud layer to produce the convective available potential energy needed for developing cumulus to overcome transition layer stability. The mesoscale regions appear to fit the description of cyclic cumulus convection proposed in a previous study, and this theory is expanded to account for diurnal variations in the stability of the transition layer. The occurrence of these mesoscale clusters of vigorous convection makes it difficult to determine if the latent heat flux in the cloud layer has actually decreased in the late afternoon and early evening, when the transition layer is the most stable.

Liquid water structure was examined and no pronounced diurnal signal was found. Results showed that clouds thicker than approximately 450 m tended to have subadiabatic integrated liquid water contents, presumably due to evaporation of drizzle in the subcloud layer, removal of liquid water at the surface, and the evaporation of cloud water at cloud top. A significant fraction of clouds less than 450 m thick produced liquid water contents that were greater than adiabatic, and there may be a physical mechanism that could produce such values in this cloud system (i.e., lateral detrainment of cloud water from convective elements mixing with existing liquid water in decoupled stratus or with liquid water detrained by nearby convective elements). Unfortunately, instrument limitations may have also produced these greater-than-adiabatic values and the extent of instrument artifacts in these results is unclear.

1. Introduction

In the Northern Hemisphere summer, the net cloud forcing over the eastern ocean margins exhibits a large meridional gradient at approximately 30°–40°N, with magnitudes decreasing toward the Tropics (Randall et al. 1984; Ramanathan et al. 1989; Harrison et al. 1990). In this latitude range, stratus beneath the subsidence inversion of the subtropical anticyclone coexist with newly formed trade cumulus having bases at a lower level (Albrecht et al. 1995a). As this marine boundary layer, with its multiple cloud types, is advected farther south by the Hadley circulation, the stratus gradually evaporate, leaving scattered trade cumulus, which allows more solar radiation to reach the ocean surface. This transition process has been simulated by Krueger et al. (1995) and Wyant et al. (1997).

Although diurnal variations in marine boundary layer clouds, precipitation, and thermodynamic structure have long been recognized, the diurnal characteristics of the transition region, where cumulus beneath stratus is a prominent cloud type, have not been fully resolved. There are several past observational studies in which the diurnal cycle of marine boundary layer structure in the transition regime has been discussed, although a comprehensive conceptual view has not yet been formulated (Betts et al. 1995; Klein et al. 1995; Miller and Albrecht 1995; Rogers et al. 1995; White et al. 1995).

Corresponding author address: Dr. Mark A. Miller, Brookhaven National Laboratory, P.O. Box 5000, Upton, NY 11973-5000.
E-mail: miller@bnlocn.das.bnl.gov

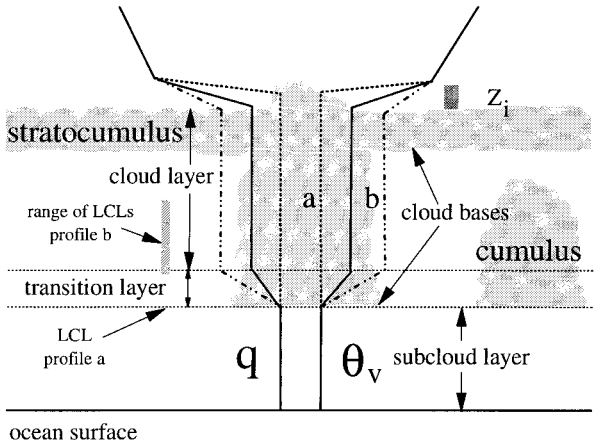

FIG. 1. A schematic diagram of three different thermodynamic profiles of the mixing ratio q and the virtual potential temperature θ_v frequently observed on Santa Maria during ASTEX. The thin dotted horizontal lines represent the approximate boundaries of the transition layer. Profile a (thick dotted line) represents the core of an undiluted cumulus updraft, whereas profile b (dot-dashed line) represents strongly decoupled cloud and subcloud layers. The solid line represents an average of these profiles. The lifting condensation levels (LCLs) for the two profiles are shown and the shaded areas represent cloud liquid water.

A complete understanding of this cycle is particularly important because the cumulus/stratocumulus cloud system is frequently observed in the summertime marine boundary layer over the northern Pacific Ocean (Klein et al. 1995), and the results of the Atlantic Stratocumulus Transition Experiment (ASTEX; Albrecht et al. 1995a) suggest that this may also be the case over the Atlantic Ocean.

In this paper, more data from ASTEX are analyzed and the diurnal cycle of cloud and thermodynamic structure in the transition region is examined. Particular attention is given to differentiating the evolution of cumulus from that of stratus when the two cloud types are coexisting, and to defining the roles of each of the constituent cloud types in modulating the characteristics of the cloud field as a whole. The data that are analyzed were collected using 3-hourly radiosonde ascents and a suite of surface-based in situ and remote sensors deployed on the island of Santa Maria during ASTEX (Miller and Albrecht 1995). The advantage of this Eulerian measurement approach is that it can provide continuous, detailed samples of the cloud field that can be linked to specific thermodynamic profiles. Presentation of new findings will follow a summary of previous studies of diurnal variability in the transition region.

2. A review of previous work

Several types of thermodynamic profile are frequently observed in the intermittently decoupled transition region boundary layer and schematic diagrams of typical soundings are illustrated in Fig. 1 (Albrecht et al. 1995b). These profiles represent conditions ranging from a single layer of stratocumulus beneath the inversion to coexisting cumulus and stratocumulus. In soundings from ASTEX, particularly those taken when the boundary layer is on the order of 1 km in depth, the lower 20%–40% of the marine boundary layer has a higher mixing ratio q and lower virtual potential temperature θ_v than the region above. This region is termed the *subcloud layer* and its upper boundary is the base of a weak inversion called the *transition layer,* which is normally found in the vicinity of the cumulus cloud base. From the top of the transition layer to the base of the trade inversion, there is a *cloud layer* that may contain intermittent cumulus convection and/or stratus near its top. It is typically assumed that the base of the transition layer is at the surface lifting condensation level (LCL), and arguments in support of this assumption can be found in Betts (1973) and Albrecht (1993). In the undiluted core of cumulus updrafts, the transition layer is undefined and cloud and subcloud layers are separated by the LCL.

Cumulus elements can form in this environment because the moist subcloud layer is a source of convective available potential energy (CAPE). The location of the LCL is critical for the conversion of this CAPE to kinetic energy because latent heat release helps parcels overcome the negative buoyancy experienced in the transition layer. Under some conditions, cumulus clouds may form at the base of the transition layer but have insufficient energy to develop vertically. In this case, if stratus are present at the top of the cloud layer, there can be two cloud layers (Fig. 1). The cumulus and stratus are not entirely independent because the cumulus convection detrains latent and sensible heat into the cloud layer (most of this heat is probably reentrained into the subcloud layer so the impact on the stratus above is probably small). In addition, the stratus can drizzle into the cumulus layer causing evaporative cooling, and holes in the stratocumulus affect the degree and distribution of radiative cooling in the cumulus layer.

If a parcel from the subcloud layer can overcome the weak inversion in the transition layer, it may saturate, reach its level of free convection, and potentially rise to the base of the trade inversion. If there is sufficient CAPE, the undiluted core of this updraft may penetrate into the trade inversion and detrain latent heat, sensible heat, and cloud water there. Otherwise, latent heat, sensible heat, and cloud water may be detrained laterally beneath the inversion, creating a layer of stratus or reinforcing one that already exists.

In this environment, the thermodynamic profile in columns containing the undiluted updrafts originating from the subcloud layer is ''coupled'' to the surface (Fig. 1, profile a). In locations far removed from the undiluted core, laterally detrained and preexisting stratus appear thermodynamically ''decoupled'' from the surface (Fig. 1, profile b), a structure initially described by Nicholls (1984). A full range of profiles between the

coupled and decoupled extremes (Fig. 1 profiles a and b) are plausible and the cloud layer does not need to have constant values of q and θ_v as a function of height. Therefore, the boundary layer in the transition region is horizontally inhomogeneous—coupled regions surrounded by decoupled ones, and hence the term ''intermittent decoupling.'' It is also important to note that this environment supports cloud bases at two levels and that large variations in cloud thickness over relatively short periods are not unusual.

The thermodynamic constraints imposed by a decoupled column dictate that stratus have cloud bases well above the LCL (Fig. 1). These stratus are formed by two processes: mechanical mixing of the decoupled column above the LCL, which results in saturation beneath the trade inversion, or lateral detrainment of cloud water from nearby convective elements. In the case of mixing stratus, the cloud base will lie at the mixing condensation level of the decoupled layer, which always lies well above the LCL. In the case of laterally detrained saturated parcels from nearby convection, the parcels must have become neutrally buoyant during their ascent, which inherently implies that the cloud layer that they form must reside above the LCL. Disagreement between the LCL and the cloud base height is used to diagnose vertically decoupled thermodynamic structure.

By analyzing radiosonde ascents from a seven-day period during ASTEX, Betts et al. (1995) suggest links between the local diurnal variation in thermodynamic structure and the radiation budget, as should be expected. They find that the boundary layer is deepest around sunrise and heats during the day with the maximum heating rate just beneath the trade inversion. They find the nighttime transition region marine boundary layer to be characterized by a well-mixed subcloud layer and a stable cloud layer, but note that the cloud layer is more stable during the early evening, a feature attributed to solar absorption during the daytime. Their data suggest that after sunset the subcloud layer cools first, followed by cooling and destabilization of the cloud layer, ''presumably because of the coupling between the cloud field and the longwave radiative cooling.''

An analysis of a long time series of ship observations from the transition region is presented in Klein et al. (1995) and used to study the structure of the transition region in the summertime eastern Pacific Ocean basin. They find a mean nighttime thermodynamic environment that is conditionally unstable but can form cumulus clouds only if rising unsaturated parcels can penetrate a thin stable layer that lies just beneath their lifting condensation level. The predominant cloud structure that they find in this thermodynamic environment is coexisting cumulus and stratocumulus with bases at different levels, and the probability of observing this particular structure increases by 10% from nighttime to the afternoon hours, although the total fractional cloudiness decreases during this period. The fractional coverage of cumulus alone and stratocumulus alone are found to be nearly out of phase, with cumulus alone more likely during the afternoon, when stratocumulus alone is less likely. Their dataset does not permit them to dissect the coexisting cumulus and stratocumulus cloud types to see how the two constituents evolve during the diurnal cycle, a subject that will be addressed in this paper.

Permanent decoupling is suggested by Klein et al. (1995) as one reason why the diurnal cycle of cloud fraction in the transition region is so great. They argue that if decoupled stratocumulus is predominantly supported by cumulus convection, it may be susceptible to breakup due to daytime reinforcement of the transition layer, which leads to a decrease in cumulus convection. Although not specifically applicable to the transition region, in a recent paper Pincus et al. (1997) present evidence in support of the hypothesis that the extent to which California stratus clouds become broken in the afternoon may depend on the optical properties of the morning clouds. Defining the physical processes that modulate observed diurnal variations in cloud fraction remains a subject of considerable debate.

Surface-based remote sensors and a plane-parallel cloud model were used by White et al. (1995) to demonstrate the radiative effects of the diurnal cycle of cloudiness in the transition region. They find significant variability in cloud structure during the diurnal cycle and show that a wide variety of convolutions are possible due to the complex boundary layer structure in the transition region. As in the other studies, they observe a decrease in the cloud fraction during the daytime.

With respect to the diurnal cycle, Rogers et al. (1995) suggest that shortwave radiation provides an environment for convection but may prohibit the development of deeper clouds during the daytime by increasing the stability near the transition layer. According to data from a nocturnal case study during ASTEX, they found that cumulus convection beneath stratocumulus can enhance the sensible and latent heat fluxes in the marine boundary layer by nearly an order of magnitude. Rogers et al. (1995) postulate that a cycle exists between cumulus development and moisture in the subcloud layer. When the mixed layer moistens sufficiently to trigger new cumulus development, moisture is quickly transported out of the subcloud layer and must be slowly replenished by the surface moisture flux. Because of this cycle, they suggest that it is likely that the boundary layer will have a water vapor distribution that is highly variable spatially. Moreover, they note the complexity of the relationship between cumulus and the latent heat flux and suggest that small cumulus may enhance the flux, but later as water vapor is redistributed vertically, the latent heat flux decreases with increased convective activity.

A characteristic of the transition region is the presence of mesoscale organization. Miller and Albrecht (1995) show that major drizzle events at the surface correspond with mesoscale patches of coexisting cumulus and stratocumulus, and they present evidence that these patches

affect surrounding decoupled regions through lateral detrainment of cloud matter and subcloud layer wakes. They further show that drizzle associated with cumulus convection conditions the subcloud layer in a manner that reinforces decoupling, an idea that is consistent with previous modeling studies (Albrecht 1993; Wang 1993).

A common process in most of these studies is the diurnal regulation of cumulus convection by the changing stability of the transition layer. This process is hypothesized to be one of the factors that controls the diurnal change in cloud fraction, a common observation in all of the previous studies. Conspicuously absent, however, are continuous measurements of the cloud structure and its relationship to the thermodynamic environment that can validate this idea. The purpose of this case study is to provide some direct evidence of this process and to briefly examine other related aspects of the diurnal cycle.

3. Instrumentation and data processing

Sensors designed to measure cloud and boundary layer structure were deployed on the northwestern coast of the island of Santa Maria in the Azores and operated for 27 days during ASTEX. This system (described in Miller and Albrecht 1995) included standard surface sensors, radiosondes, a Vaisala laser ceilometer (model CT 12K), a 4-channel microwave radiometer, and a 94-GHz radar.

An important component of the instrument package was the zenith-pointing, 94-GHz cloud-sensing radar. Unlike optical remote sensors, its transmitted pulse penetrates clouds and light precipitation, allowing continuous measurement of cloud-top height and diagnosis of cloud internal structure (Lhermitte 1987; Clothiaux et al. 1995). During ASTEX, the clouds were sampled every 5 seconds with this radar, and 30-s averages of these data are used in this study. A complete description of the radar and the algorithm used to determine the cloud-top heights from the reflectivity profile is found in Clothiaux et al. (1995). One modification to the algorithm used to determine the cloud-top height from the reflectivity profile was necessary when significant drizzle was observed in the cloud and subcloud layers. In this circumstance, the radar was found to overestimate the cloud-top height due to the configuration of the receiver electronics. This problem was manifested as regions of false weak echoes above cloud top, particularly when the cloud was drizzling, and an additional step was added to the algorithm to account for this problem.

A comparison of the cloud-top heights measured by the 94-GHz radar and the top of the saturated layer detected by 32 Vaisala Model RS 80 radiosondes launched from the radar site was completed for a subset of the ASTEX data. These types of radiosondes occasionally underestimate the in-cloud relative humidity and can be influenced by solar radiation, although these errors do not significantly impact the ability of the radiosonde to identify the strong gradients at the base of the trade inversion. Since the cloud structure was often complicated, if an individual radiosonde ascent was found to disagree strongly with a half-hour average of the radar-measured cloud top, the 30-s cloud-top measurements were consulted. If multiple cloud layers were found, the cloud top that most closely matched the radiosonde cloud top was accepted, although this subjective determination was necessary in only 3 of the 32 comparisons. The average radiosonde and radar cloud tops were both found to be 925 m, but the root-mean-square difference between the two measurements was 98 m. These values seem reasonable given that the resolution volume of the radar was 75 m. In addition, very thin clouds may be undetected by the radar while they are sampled by the radiosonde, and there are differences in the volumes sampled by the two instruments. In summary, the cloud-top heights from the 94-GHz radar determined with the modified algorithm appear to be reliable.

A zenith-pointing, 4-channel, microwave radiometer operating at frequencies of 22, 24, 31, and 50 GHz was used to passively monitor the vertically integrated water vapor and liquid water contents. This radiometer sampled at a rate of 26 seconds through a beamwidth of 5°. The vertically integrated liquid water contents were computed by combining data from the 24-GHz and 50-GHz channels because this combination has a minimum detectable liquid water content of $\sim$0.05 mm, which is lower than other channel combinations. The occurrence of liquid phase mid- and high-level clouds can complicate the interpretation of these radiometer data, but these clouds generally contain predominantly ice and relatively little liquid water when compared to marine boundary layer clouds and precipitation. Thus, it is assumed that the bulk of the vertically integrated liquid water measured during the 3-day study period is contained in the marine boundary layer.

To ensure that the boundary layer measurements used in this study are representative of the cloud system over open ocean, a stringent conditional sampling strategy was developed to minimize potential island influences. The island of Santa Maria, which has a maximum dimension of $\sim$15 km, lies in the wake of the larger island of San Miguel, so an acceptable sampling criterion must ensure that the effects of both islands are properly filtered. In addition to potential island influences, the observations must be categorized according to the synoptic flow so that those applicable to the climatologically dominant Azorian high pressure system are separated from those associated with other synoptic features. All these factors suggest that one important sampling criterion is the wind direction, and consequently the scheme outlined in appendix A was devised. Out of a possible 648 hours of available data, 218 hours (33.6%) were found not to be acceptable and only 176 hours (27%) had a northeasterly wind component represen-

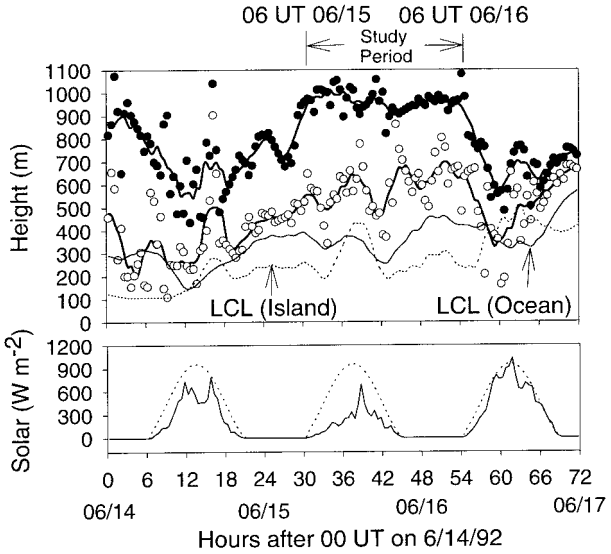

FIG. 2. (a) A 3-day time series of half-hour averages of cloud-top height (filled circles), lowest cloud-base height (open circles), and 3-h running averages of these variables (thick solid lines). The 3-h running average of the island LCL (dashed line) and ocean LCL (thin solid line) are indicated. (b) The broadband solar radiation at the surface site (solid line) and in clear-sky conditions (dotted line). The 24-h study period used to diagnose the diurnal cycle is indicated.

tative of the climatological mean flow in the region. Of this 176 hours, the longest period of continuous data was 72 hours (3 days), so that period was chosen for analysis.

Conditional sampling by wind direction alone is insufficient to eliminate island influences, a fact that is easily demonstrated by analyzing the 3-day time series described above. To illustrate that the depth and cloud coverage of the boundary layer are also important, the time series of cloud top, lowest cloud base, and LCL are plotted in Fig. 2. A representative oceanic LCL can be computed from a combination of island and ship data, as discussed in Miller and Albrecht (1995), and this LCL along with the island LCL are plotted to demonstrate how island influences are manifested in the data. The island LCL is lower at night due to radiational cooling of the sandy surface and higher during the day due to solar heating. Consequently, a layer of very low stratus can form over the island, beneath the marine boundary layer clouds, when the boundary layer is moist enough and the island surface is cool enough. Such stratus layers are observed on the mornings of 14 and 16 June, when the cloud base is found near the island LCL and beneath the ocean LCL. On 16 June, at times the 3-h running average island LCL does not show good agreement with the half-hour average cloud base heights, but the raw half-hour island LCLs (not shown) agree quite well with the half-hour average cloud base heights.

Strong solar heating of the island surface can drastically affect the cloud structure when the boundary layer is shallow ($<$600 m), and rapid changes in cloud-top and cloud base height are seen during the afternoon on 14 and 16 June. The surface irradiance (Fig. 2b) shows more solar radiation reaching the island surface on these two days than on 15 June. A contour plot of the potential temperature for these days (not shown) shows a strong correlation between changes in the cloud structure on 14 and 16 June and the development of a deep internal boundary layer over the island. In contrast, data from June 15 do not show a well-defined response to solar heating, perhaps because less solar radiation is reaching the surface and the boundary layer is deeper. Consequently, daytime data from only 15 June will be used to study the diurnal variability of cloud structure, although data from all three days will be used to demonstrate the effects of synoptic scale variability.

The cloud fraction, cloud boundaries, vertically integrated cloud liquid water contents, surface rainfall rate, and surface mixing ratio are used in this paper to describe the state of the cloud structure. The clouds above the Santa Maria surface site were sampled at a resolution of 30 s or less by the narrow-beam, zenith-pointing instruments. For many of the analyses, averages and statistics are computed for half-hour periods. Three-hour running means of these half-hour averages are used when cloud boundary data are being compared with the thermodynamic structure, which was sampled every 3 h. Statistics of the raw 30-s measurements of cloud base height are also used in one of the analyses to help quantify details about the cloud base structure on cloud scales. Thus, the analyses below scan a range of temporal scales from 30 s to 3 h.

4. Results

A cross section of the mixing ratio in the lower 3 km of the troposphere for the 3-day period, overlaid with 3-h running averages of the cloud-top height and the lowest cloud base height, is shown in Fig. 3. The lowest cloud base height is used because the ceilometer cloud base height selection algorithm can detect two cloud base heights when a thin cloud layer is located below the base of a higher cloud layer. This figure demonstrates the variability of the boundary layer depth on relatively short timescales in the transition region as a result of a combination of island effects and synoptic variability. The mixing ratio cross section is used in this example because it shows an important characteristic of the study period: well-defined drying above the inversion after about 1800 UTC 14 June (hour 18 in Fig. 3). Associated with this drying are rapid changes both in the depth of the marine boundary layer between 1800 UTC 14 June and 0600 UTC 15 June (hours 18–30 in Fig. 3) and in its vertical thermodynamic structure from nearly well mixed to intermittently decoupled. This fundamental change has an important impact on the cloud structure.

The effect of this drying on the cloud structure is illustrated by separating the cloud data into coupled and decoupled components. To separate the cloud types it

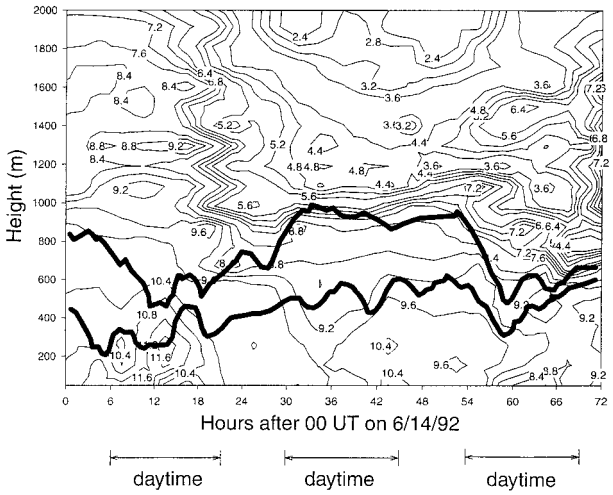

FIG. 3. Time–height cross section of the mixing ratio q (g kg^{-1}) calculated from radiosonde data at Santa Maria from 0000 UTC 14 June through 0000 UTC 17 June. The thick black lines are 3-h running averages of the cloud top and lowest cloud base.

is assumed that the bases of cumulus clouds are near the LCL, and to avoid the effects of measurement error an envelope of ± 100 m surrounding the LCL is used as an acceptance criterion for coupled clouds. One source of measurement error during this 72-h period is calculation of a representative LCL. Air temperature data collected from a nearby research ship are only available on 15 June and the mean of these temperature data are used, along with the island mixing ratio, to compute the LCL during the 72-h period. Because the separation between cumulus and stratus cloud bases is typically quite large and the ocean surface temperature is reasonably constant over a 3-day period, the use of this acceptance envelope is not likely to alter the results in any meaningful way. The 30-s observations were processed for the period between 1800 UTC 14 June and 0600 UTC 15 June (hours 18–30 in Fig. 3) during the period of maximum drying above the inversion, and the clouds classified into coupled and decoupled components (Fig. 4).

When the total fractional cloud coverage during this period is plotted against cloud-top height (a good indicator of z_i), a weak linear relationship exists between the two variables as indicated by the low value of r^2 (0.44). When the fractional coverage of decoupled clouds is plotted, however, a strong linear relationship is found ($r^2 = 0.81$), and a strong linear relationship is also indicated between the fractional coverage of coupled clouds and the boundary layer depth ($r^2 = 0.74$). The cloud structure over a period of a few hours changes in a predictable way in response to deepening of the marine boundary layer and drying above the boundary layer, but this structural modification is not related to the diurnal cycle and must be filtered before the true nature of the cycle can be revealed.

It is apparent from Figs. 3 and 4 that attempts to study

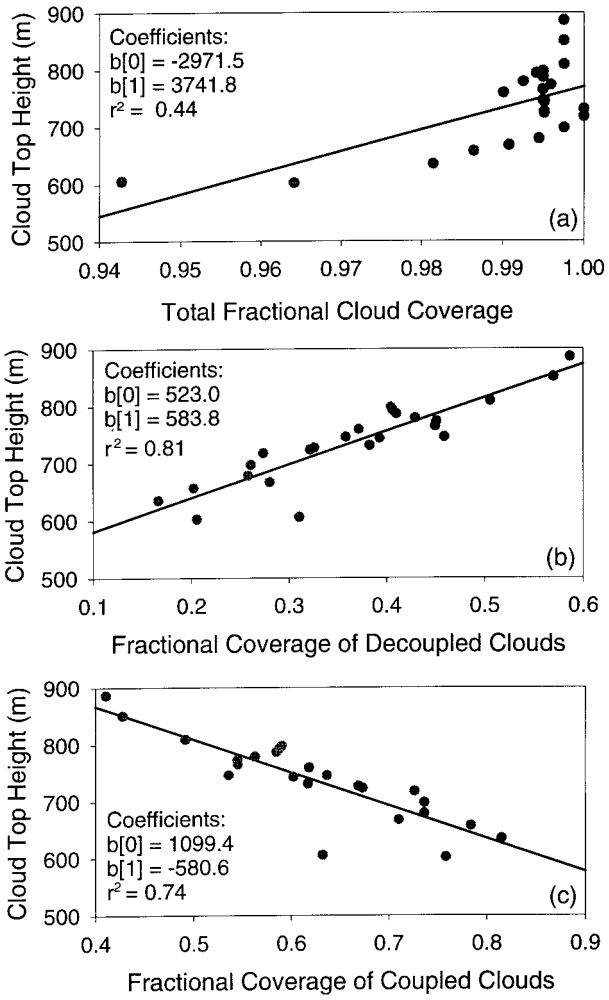

FIG. 4. Cloud-top height (or boundary layer depth) vs fractional cloud coverage from 1800 UTC 14 June to 0600 UTC 15 June: (a) all clouds, (b) decoupled clouds (bases >100 m above the LCL), and (c) coupled clouds (base heights within ± 100 m of the LCL). The solid lines are linear regressions and the coefficients for each line are indicated along with the square of the correlation coefficient.

the diurnal variations in the cloud structure by averaging data from the 3-day study period are destined to fail because of synoptic variability and afternoon island effects (14 and 16 June). As a result, the 24-h period beginning at 0600 UTC on 15 June is chosen for analysis because the depth of the boundary layer is relatively constant. This time series overlaps a portion of that used by Miller and Albrecht (1995) to examine mesoscale processes in the transition region; estimates of the horizontal scales of observed regions of cumulus activity, as well as some of the discrete soundings used in this analysis, are found there.

a. Thermodynamic structure

The thermodynamic evolution of the boundary layer during the 24-h study period can be illustrated by over-

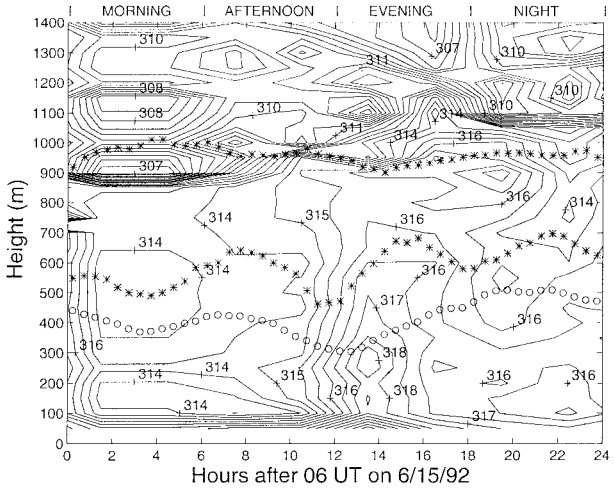

FIG. 5. Time–height cross section of the radiosonde equivalent potential temperature θ_e (K) at Santa Maria from 0600 UTC 15 June through 0600 UTC 16 June. The asterisks represent 30-min values of the 3-h running average of the cloud-top height and lowest cloud-base height measured by surface-based remote sensors. The open circles are the over-ocean surface LCL.

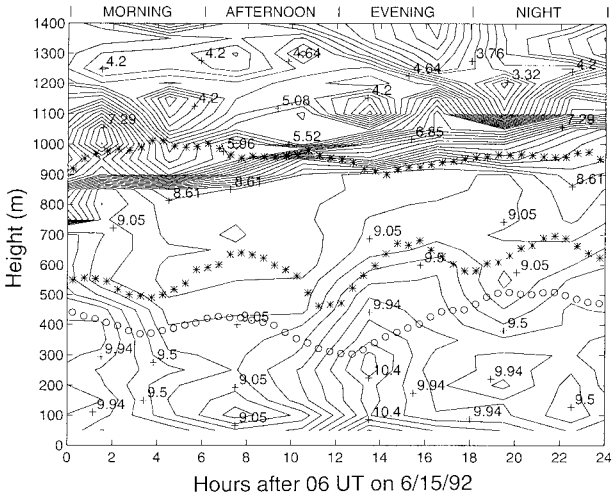

FIG. 6. As in Fig. 5 but for mixing ratio q (g kg^{-1}).

laying the 3-h running averages of measured cloud structure with contours of θ_e (Fig. 5), q (Fig. 6), and θ_v (Fig. 7) calculated from data collected during the 3-hourly radiosonde ascents. There are two short periods during which radar cloud-top data are not available, so interpolations from surrounding data are used to compute the 3-h running mean. As suggested in Betts et al. (1995), caution must be used in interpreting the radiosonde moisture data during the middle of the day because the Vaisala Humicap sensor is subject to heating errors. During the study period, the cloud fractional coverage is quite large (>90%), so the radiative heating of the humicap sensor may not be as severe as that found by Betts et al. (1995).

Because θ_e is conserved in moist adiabatic processes, its structure can highlight changes in the thermodynamic structure related to mixing and the radiative fluxes (Fig. 5). For example, during the morning and early afternoon hours, the maximum gradient in θ_e lies beneath the measured cloud top, while during the evening and night it lies well above it. The variability in θ_e at cloud top is modulated by changes in the mixing ratio (Fig. 6) and virtual temperature (Fig. 7). During the morning and most of the afternoon, the thin layer at cloud top is warmer and drier than during the evening and night. One possible explanation for this offset between the gradient in θ_e and the cloud-top height is variable mixing processes at cloud top.

There is drying in the cloud layer during the daytime as illustrated in Fig. 6 by the drop in elevation of the 9.05 g kg^{-1} contour line around 0900 UTC (hour 3 in Fig. 6) and warming in the late afternoon as illustrated in Fig. 7 by the drop in elevation of the 291.8-K contour starting near 1400 UTC (hour 8 in Fig. 7). The value of θ_e in the cloud layer does not change much during the daytime because the drying is offset by warming. The highest values of θ_e in the subcloud layer are measured during the late afternoon and early evening in association with an increase in moisture of over 1 g kg^{-1} in the subcloud layer.

The stability of the marine boundary layer with respect to unsaturated ascent is evaluated from the cross section of virtual potential temperature, θ_v (Fig. 7). Little diurnal variability in θ_v is observed at the trade inversion during the 24-h period, except after 0200 UTC 16 June (hour 20 on the plot) when a clear change in the above inversion conditions is indicated. Within the boundary layer, the vertical gradient of θ_v in the vicinity of cloud base increases during the afternoon, signifying increasing stability in the transition layer. The transition layer is deep and ill defined during the morning and becomes well defined and the most stable around sunset.

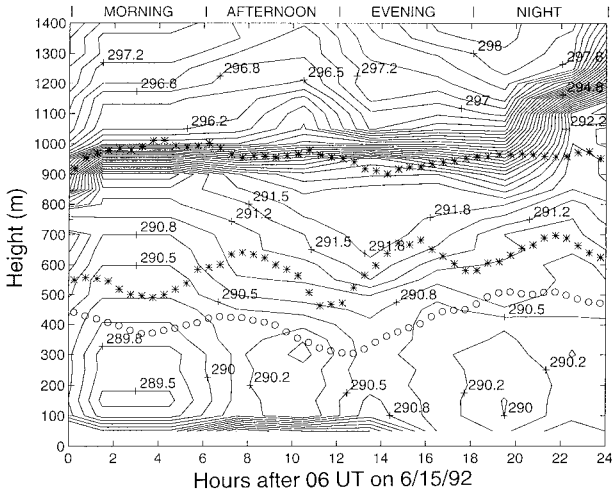

FIG. 7. As in Fig. 5 but for the virtual potential temperature θ_v (K).

During the study period, the 3-h moving average cloud-top height (Figs. 5–7) exhibits relatively steady behavior, while large variability in the 3-h moving average lowest cloud base height is observed, reflecting complex cloud structure with bases at two levels. The 3-h running mean LCL consistently lies below the 3-h running mean cloud base height because decoupled clouds are present in the cloud field throughout the diurnal cycle. Since the 3-h running mean cloud base height lies somewhere between the 3-h running mean of the cumulus and decoupled stratocumulus cloud base heights, specific details about the cloud structure are not well quantified using this moving average but are quantified below using higher resolution data. It is noteworthy, however, that the movement of the 3-h running mean lowest cloud base height is well correlated with that of the 3-h running mean LCL, suggesting that the location of the LCL is intimately tied to the structure of the cloud base as expected.

b. Cloud structure

The 3-h running averages of cloud structure are compatible with the resolution of the radiosonde data but smear important details about the structure of the cloud field on shorter timescales. The half-hour averages of the average cloud-top height, cloud base height, and LCL are presented in Fig. 8, along with the half-hour standard deviations of these variables. Three-hour running means from the earlier analyses are shown for comparison. There are two periods (0900 UTC and between 2100 and 2300 UTC 15 June) when the radar cloud-top measurements are not available, so these data are excluded from the analysis. To characterize drizzle and solar radiation, half-hour averages of the surface drizzle rate from the optical rainguage and solar radiation from a broadband solar radiometer are included in Fig. 8. Clear-sky solar radiation is determined by using a polynomial fit to data taken during three clear days during ASTEX (9, 10, and 19 June) and are provided as a reference for the cloud statistics.

In theory, the cloud bases of coupled cumulus elements should lie at the LCL, assuming the subcloud layer is well mixed. Defining all clouds with bases near the LCL as being coupled does not permit a distinction between the well-mixed stratocumulus and cumulus cloud types, but this caveat does not impair the results of the current study because no well-mixed stratocumulus clouds are observed during the 24-h study period. In practice, the subcloud layer is not always well mixed and is subject to modifications from penetrating downdrafts and evaporating drizzle (Miller and Albrecht 1995). This complication thwarts efforts to link specific 30-s cloud base observations with 2-min measurements of the LCL (interpolated to 30-s resolution). Since the processes that lead to a subcloud layer that is not well mixed occur on relatively short timescales (less than a half-hour), another approach is to use the maximum and minimum values of the LCL during the half-hour as an acceptance envelope for the identification of coupled clouds. This is the approach that is adopted in the analysis to follow.

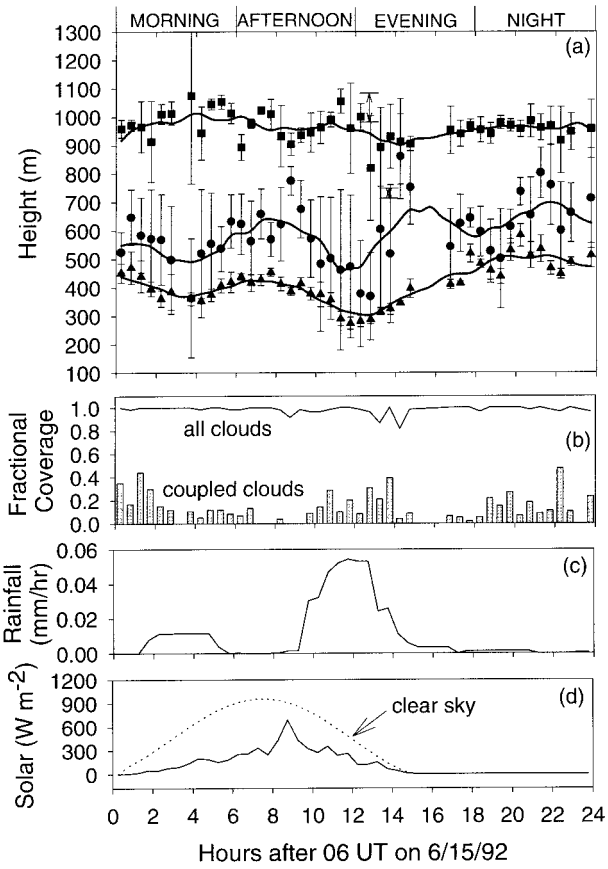

FIG. 8. Time series at Santa Maria from 0600 UTC 15 June through 0600 UTC 16 June. (a) Half-hour averages of cloud-top height (filled squares), cloud base height (filled circles), over-ocean surface LCL (solid triangles), standard deviations of these variables (bars), and 3-h running averages (solid lines); (b) fractional coverage of all clouds (solid line) and coupled clouds (bar graph) with bases within the envelope of the half-hour standard deviations of the over-ocean LCL; (c) half-hour averaged surface rainfall rate in mm h^{-1}; and (d) broadband solar radiation at the island surface in watts per square meter (solid line) and under clear skies (dashed line).

The cloud-top height is generally higher and more variable during the daytime than during the night (Fig. 8a). This variability is observed over periods of an hour or two, as well as on scales of less than one-half hour, and is due to strong convective elements, perhaps penetrating the inversion, surrounded by thin patches of stratocumulus. Periods of enhanced variability at cloud top correspond reasonably well with minimum values of the LCL modulated by water vapor accumulation (Fig. 6) in the subcloud layer. When the subcloud layer moistens, CAPE is increased, which strengthens the updrafts in these daytime and early evening convective clouds.

The half-hour standard deviations of cloud base

height (Fig. 8a) show variations of up to 400–500 m, particularly during periods when the LCL is low. Lowering of the LCL results in a decrease in the cloud base heights of coupled cumulus elements. There are periods when the standard deviation of cloud base height extends well below the range of measured LCLs during the half-hour. These incidents are well correlated with the occurrence of heavy drizzle in the subcloud layer (Fig. 8c) and suggest that the some of the cloud base heights selected from the ceilometer reflectivity profile during these periods are erroneous. Therefore, the coupled-cloud detection algorithm does not count cloud bases below the minimum LCL (lower bound of the acceptance envelope) during the half-hour as coupled but rejects them as questionable observations.

The fractional coverage of both coupled clouds and all clouds (including coupled clouds) shows diurnal variability (Fig. 8b). It is tempting to conclude that the coupled clouds exhibit semidiurnal variability, but missing data during the evening hours contribute to the second minima. In addition, the fractional coverage of coupled clouds during the afternoon periods of heavy drizzle are potentially biased low by errors in the ceilometer cloud-base selection algorithm, which leads to rejection of the data. Considering all potential instrument limitations and the nature of the radar echoes during the study period, it seems likely that the fractional coverage of coupled clouds is lower during daytime than at night, although there is a period during the late afternoon when the coverage of coupled clouds is temporarily enhanced.

Precipitation at the surface (Fig. 8c) shows two well-defined maxima, one in the morning and one in the late afternoon, both associated with decreases in the LCL and increases in the variability of the cloud boundaries. These observations suggest that convection is the deepest and strongest during these periods. Because the subcloud layer is more moist during the late afternoon and early evening, CAPE probably reaches a maximum at this time, which accounts for the strength of the convective elements during that period and their increased surface drizzle production. A few hours after sunset, the stability in the transition layer decreases. Hence, coupled clouds can form more easily and the fractional coverage of coupled clouds increases. Radar echoes indicate that drizzle is present throughout the boundary layer during the late evening and night, which may act to reinforce decoupling during the nighttime period. Surface drizzle is not observed during the night, perhaps because evaporation in the subcloud layer is increased and updraft velocities in the cumulus elements are decreased.

Because the cloud structure is so complex, detailed characteristics of this structure are best resolved using frequency distributions of the 30-s observations. The 30-s values of the lowest cloud base height (laser ceilometer), highest cloud-top height (94-GHz radar), and cloud thickness (combined data from both sensors) are grouped into height bins and plotted as frequency distributions for four time segments during the 24-h study period: morning, afternoon, evening, and night. The cloud base heights and cloud-top heights are binned according to the vertical resolution of the measurements, which are 15 and 75 m, respectively, and the results of this analysis are shown in Fig. 9. For each of the four 6-h periods, the mean and the range of the 2-min LCLs are plotted, along with the mean values of the cloud boundary heights.

The frequency distributions of cloud base height (Fig. 9) show bimodal structure during the morning and afternoon and multimodal structure during the evening and night. The cloud-base height frequency distribution during the morning hours has two prominent peaks: a relatively narrow peak at ~700 m and a broader peak at 400–550 m. The separation of the two cloud base height distribution peaks during the morning and afternoon is associated with the presence of distinct cumulus and decoupled stratocumulus cloud layers with a significant difference in cloud base height. From morning to afternoon, the peak in the distribution associated with the decoupled stratocumulus increases slightly and the peak broadens upward toward cloud top. During the same period, the mean cloud-top height decreases. These results suggest that the decoupled stratocumulus are becoming thinner from morning to afternoon. The distribution of cloud base heights exhibits the widest range toward evening when some cloud base heights are above 900 m (Fig. 9c). Commensurate with this wide range in the cloud base height distribution is an increase, as compared to the afternoon hours, in the cumulative frequency of cloud base heights that fall within the range of observed 2-min LCLs for the 6-h evening period. This result suggests an increase in the fractional coverage of coupled clouds during the evening, in agreement with the analysis presented in Fig. 8. This trend of increasing coverage of coupled clouds continues into the nighttime period.

Inspection of the cloud-top height histograms in Fig. 9 show cloud-top heights well below the top of the boundary layer during the afternoon (between 600 and 700 m), evening (between 400 and 500 m), and night (between 600 and 750 m). During the morning, the cloud-top height is always near the top of the boundary layer. There are at least three feasible explanations for this observation: 1) the decoupled stratus layer at the top of the boundary layer is thick during the morning, increasing the likelihood that even shallow cumulus cloud tops will merge with the stratus above, thereby not leading to a distinct cumulus cloud top; 2) the transition layer is more stable during the afternoon and evening, which may limit the growth of some convective elements; and 3) the reduction in CAPE during the night may prohibit many clouds from reaching the stratus layer.

To demonstrate the diurnal variability of the vertical extent of cloud liquid water in the boundary layer, cloud thickness histograms for morning, afternoon,

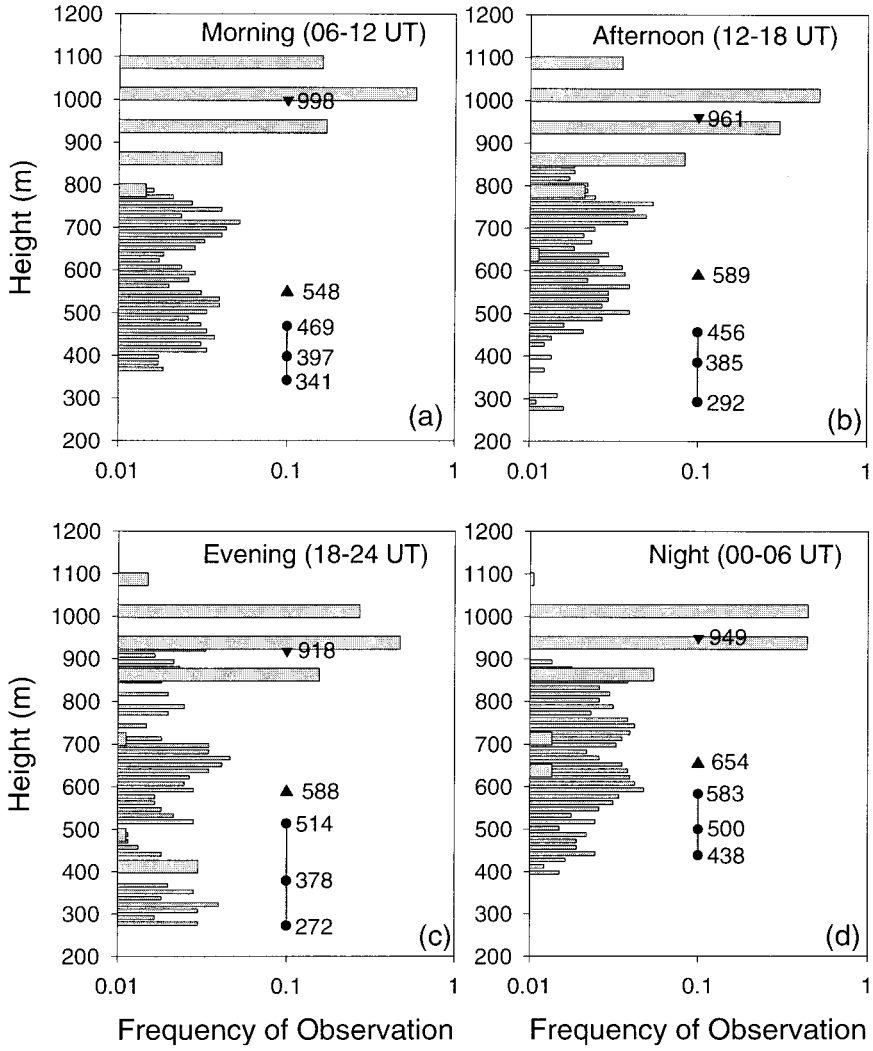

FIG. 9. Frequency distributions of cloud base height (15-m bins; thin bars) and cloud-top height (75-m bins; thick bars) for four 6-h periods representing (a) morning, (b) afternoon, (c) evening, and (d) night. The mean cloud base heights and cloud-top heights are indicated with filled and inverted triangles, respectively, and the 6-h mean LCL, along with the maximum and minimum LCLs during the period, are shown as filled circles.

evening, and night are shown in Fig. 10. The cloud thickness is computed by summing the thickness of each cloud layer below the trade inversion. Note that subtracting the mean cloud base height from the mean cloud-top height (Fig. 9) does not account for the existence of separate cloud layers. The cloud thickness results (Fig. 10) show that the clouds are the thickest during the morning and thin during the afternoon, evening, and night. During the morning, there are few clouds thinner than 200 m in the boundary layer, as compared to the number of thin clouds observed during the other periods. In contrast, there are no clouds thicker than 700 m during the night, while there are significant fractions of these deeper clouds during the other periods.

c. Liquid water structure

Cloud liquid water structure is examined using a combination of cloud boundary measurements from the laser ceilometer and 94-GHz radar and measurements of the integrated liquid water content from a multichannel microwave radiometer. Saturated parcels rising adiabatically through a specified vertical distance produce a known quantity of liquid water, the adiabatic liquid water content, which can be integrated through the depth of the parcel ascent to yield the integrated adiabatic liquid water content. The method used to compute the integrated adiabatic liquid water content is given in appendix B. The adiabatic liquid water content, which represents the theoretical upper bound on cloud liquid

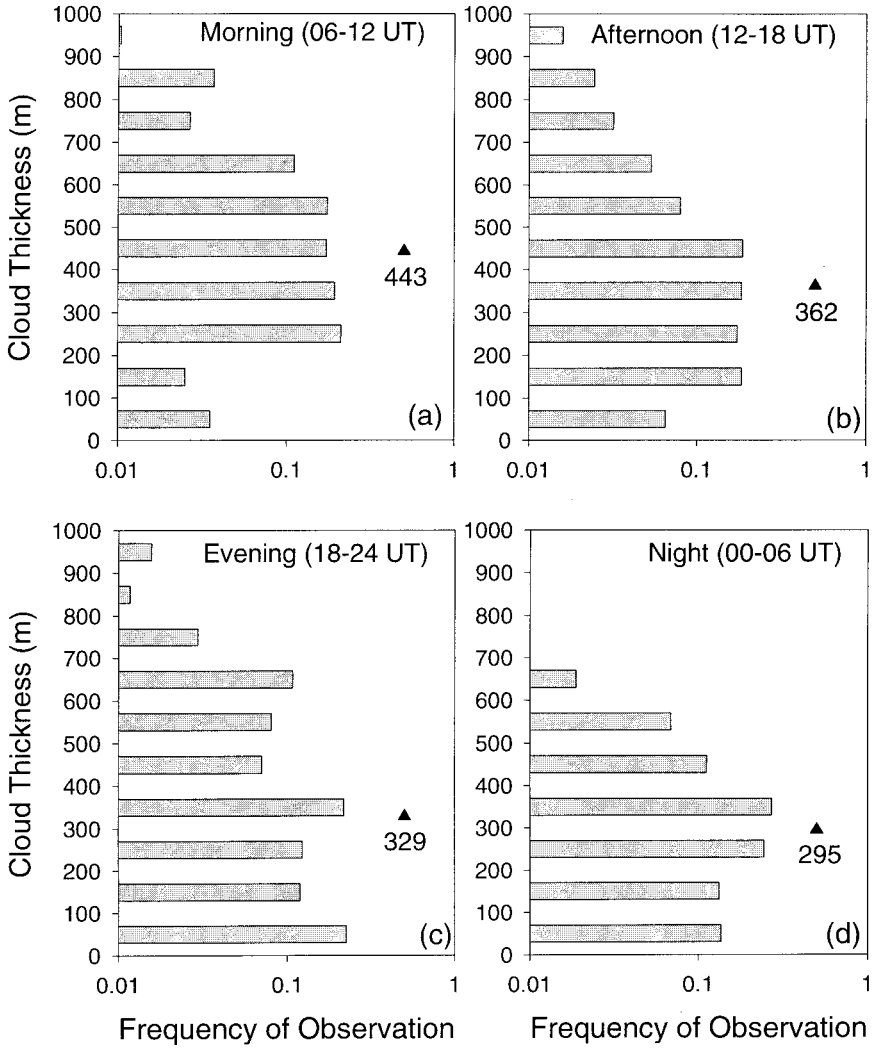

FIG. 10. Frequency distributions of cloud thickness (100-m bins) for four 6-h periods representing (a) morning, (b) afternoon, (c) evening, and (d) night. The mean cloud thickness is indicated with a filled triangle.

water for a rising parcel, is compared with the measured integrated liquid water content from the microwave radiometer. This technique was developed by Albrecht et al. (1990) and used to show that the integrated liquid water content of marine stratus off the California coast is adiabatic for most observations and subadiabatic for a few others. The subadiabatic liquid water contents were linked to the evaporation of drizzle in the subcloud layer in that study.

Relationships between cloud thickness and the integrated liquid water content for all clouds measured during the 24-h study period are presented in Fig. 11 for morning, afternoon, evening, and night. These data do not exhibit a pronouced diurnal cycle. Note that the thicker clouds have subadiabatic integrated liquid water contents, whereas the thin clouds (>450 m) often have liquid water contents that are greater than adiabatic.

Separating coupled and decoupled cloud types (Fig. 12) shows that the majority of coupled clouds are thicker than their decoupled counterparts. These thick coupled clouds produce drizzle that evaporates in the subcloud layer or is removed at the surface, which may account for the numerous subadiabatic integrated liquid water contents in these clouds. This observation is somewhat reassuring because the undiluted cores of cumulus elements rising from the LCL approximate the assumptions used in the calculation of the adiabatic integrated liquid water content. Decoupled clouds, on the other hand, account for the vast majority of integrated liquid water contents that are greater than adiabatic.

If the greater-than-adiabatic integrated liquid water contents are the result of lateral detrainment of liquid water into existing stratus, the clouds that possess this quality should have cloud bases near the top of the boundary layer. Accordingly, the observed integrated liquid water contents were sorted by cloud thickness

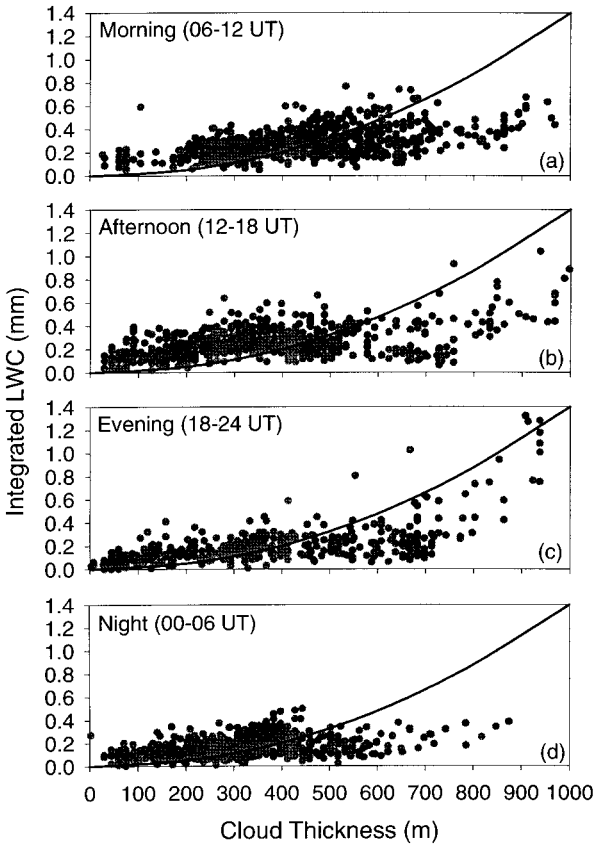

FIG. 11. Scatterplots of cloud thickness vs integrated liquid water content for (a) morning, (b) afternoon, (c) evening, and (d) nighttime clouds. The solid lines represent the adiabatic integrated liquid water contents computed with a parcel ascent model and the thin straight lines are linear fits to the data for reference.

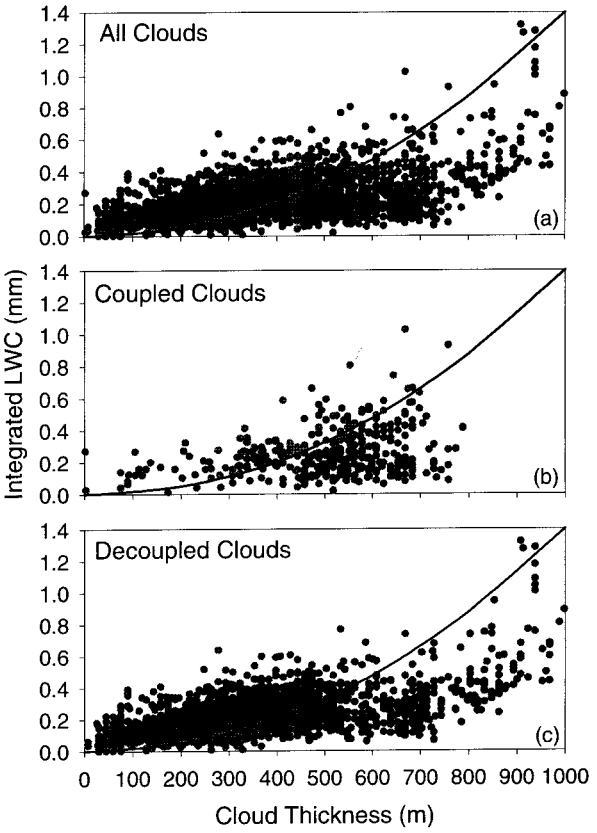

FIG. 12. Scatterplots of cloud thickness vs integrated liquid water content for (a) all clouds, (b) clouds with bases falling between the maximum and minimum values of the LCL observed within a half-hour envelope (coupled), and (c) clouds with bases above the maximum values of the LCL observed within a half-hour envelope (decoupled). The solid lines represent the adiabatic integrated liquid water contents for clouds of the specified thickness computed with a parcel ascent model.

and plotted as a function of cloud base height, along with the envelope of feasible integrated adiabatic liquid water contents for the specified range of cloud thickness (Fig. 13). As Fig. 13 illustrates, clouds less than 400 m thick near the top of the boundary layer account for the majority of the greater-than-adiabatic observations, whereas clouds thicker than 600 m are rarely greater than adiabatic and are often subadiabatic.

The findings illustrated in Figs. 11–13 are sensitive to errors in the liquid water contents, the cloud base heights, and the cloud-top heights derived from microwave radiometer, laser ceilometer, and 94-GHz radar measurements, respectively. We estimate the accuracy of the microwave radiometer retrievals used in this study to be on the order of approximately 30% with a bias of 0.03 mm of liquid water, which was corrected. Laser ceilometer estimates of cloud base height during drizzle are also prone to errors. Finally, the resolution of the 94-GHz radar was 75 m so that an error of three radar range bins leads to an error in cloud top height of 225 m. Since it is impossible to quantify these errors, it is impossible to provide rigorous error estimates for the results in Figs. 11–13. Nonetheless, the trends evident in these figures are striking and the possibility cannot be discounted that some of the observations are accurately portraying the liquid water stucture.

5. Discussion and conclusions

Changes in cloud structure through a diurnal cycle were diagnosed during a period when the boundary layer depth was reasonably constant and above-inversion conditions were relatively quiescent. Based on the measured average wind speed at the island surface of $\sim$7 m s^{-1} during the 24-h study period, the characteristic horizontal advection scale was $\sim$600 km and there were scattered high clouds over the region. The boundary layer was frequently deeper at Santa Maria during ASTEX ($\sim$1300 m) than during the study period ($\sim$950 m), and the afternoon decrease in cloud fractional coverage was less than that observed in other studies. Quantifying the synoptic-scale variability during ASTEX is a significant problem, as discussed by Betts et al. (1995). A further complication is the presence of the large island

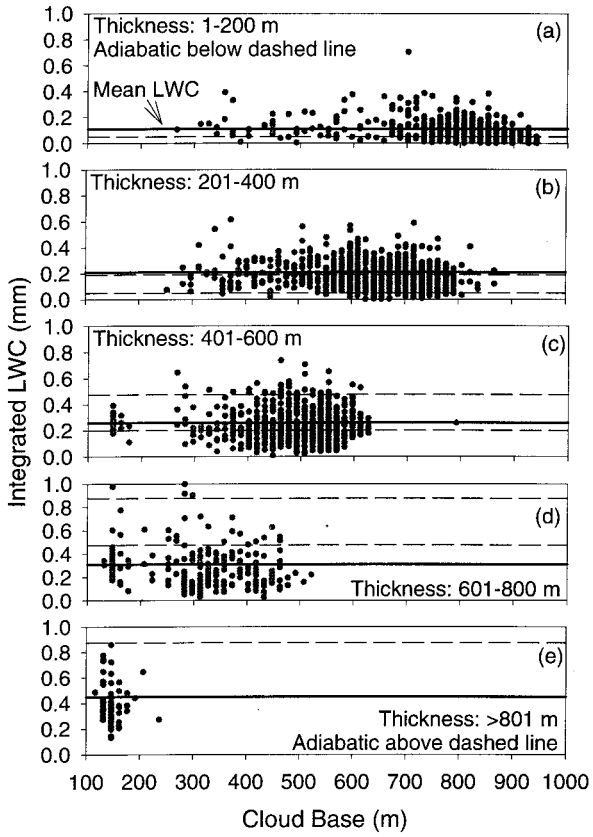

FIG. 13. Scatterplots of cloud base height vs integrated liquid water content for clouds with thicknesses of (a) 1–200 m, (b) 201–400 m, (c) 401–600 m, (d) 601–800 m, and (e) >801 m. The dashed lines represent the envelope of possible adiabatic values of integrated liquid water content for clouds of this thickness range computed with a parcel ascent model. The bottom boundary of the adiabatic envelope in (a) is the axis and the top boundary in (e) is above 1.0 mm. The solid horizontal lines represent the mean integrated liquid water contents for the data in each plot.

of San Miguel ~80 km to the north, which may have some influence on the local subsidence rate at Santa Maria. Hence, the subsidence rate at Santa Maria is difficult to determine and its impact on the results of this study are unknown.

A schematic diagram of the diurnal cycle of cloud structure observed during the 24-h study period is shown in Fig. 14. As the schematic illustrates, the thermodynamic profile is intermittently decoupled through the diurnal cycle and the transition layer is the most stable during the late afternoon and early evening. The subcloud layer always has some CAPE and the LCL is always near the transition layer, so cumulus are present throughout the diurnal cycle. Conditions are such that the region beneath the trade inversion is near saturation and a layer of stratocumulus is almost always present. Hence, there are cloud bases at two levels throughout the 24-h study period.

Cumulus activity showed a peak at about sunrise, followed by a 75% decline in fractional coverage (0.4 to 0.1) until late afternoon, when a second peak in activity was observed. A steady increase in the stability of the lower portion of the cloud layer began during the late morning hours and continued until sunset, and a 6% decrease in the total cloud fraction was observed during the period. This decrease in total cloud fraction was not well correlated with changes in the fractional coverage of cumulus convection. Because other studies consistently show daytime decreases in total fractional cloudiness on the order of 20%–30% during ASTEX, it is possible that the increase in convective activity observed during the late afternoon in this study prevented the total cloud fraction over the instrument site from decreasing.

The diurnal cycle in the thermodynamic profile corresponds to observable changes in the accompanying cloud and precipitation structure (Fig. 14). At night, echoes from the 94-GHz radar show numerous weak cumulus elements rising into a thick drizzling deck of stratocumulus. These nighttime clouds produce light precipitation that falls into the subcloud layer, but is too light to be measurable at the surface. The cumulus do not overshoot the inversion at night because there is insufficient CAPE, whereupon they laterally detrain significant amounts of their liquid water beneath the trade inversion. Evaporating subcloud drizzle reinforces decoupling during the night.

At sunrise, the cloud layer begins to warm and dry and the stability of the transition layer begins a steady increase. The evolution of observed cloud structure supports the fundamental idea that the stability of the transition layer regulates the latent heat flux in the upper part of the boundary layer, primarily by controlling the development of spontaneous cumulus convection. In the simplest possible situation, the stability near the transition layer would increase during the daytime, reducing convective activity and thereby decreasing the latent heat flux at the top of the boundary layer. This reduction would cause the cloud fraction to decrease, as discussed by Klein et al. (1995), and allow the cloud fraction to be specified as a function of transition layer stability, which is essentially the case in some current models.

The data presented in this study suggest a potential complication to this theory in the form of outbreaks of vigorous, organized mesoscale convection, especially during the late afternoon and early evening, which may form in the manner postulated by Rogers et al. (1995). According to this hypothesis, cumulus clouds develop when the mixed layer moistens sufficiently to trigger them. Accumulation of moisture in the subcloud layer (Fig. 6) is observed during the afternoon along with a pronounced increase in convective activity (Fig. 8). Both features develop and disperse relatively quickly.

The Rogers et al. (1995) hypothesis can be modified to include diurnal variability. Because the stability of the transition layer is the greatest during the afternoon and early evening, it is likely that these periods will be favored for outbreaks of vigorous, organized mesoscale

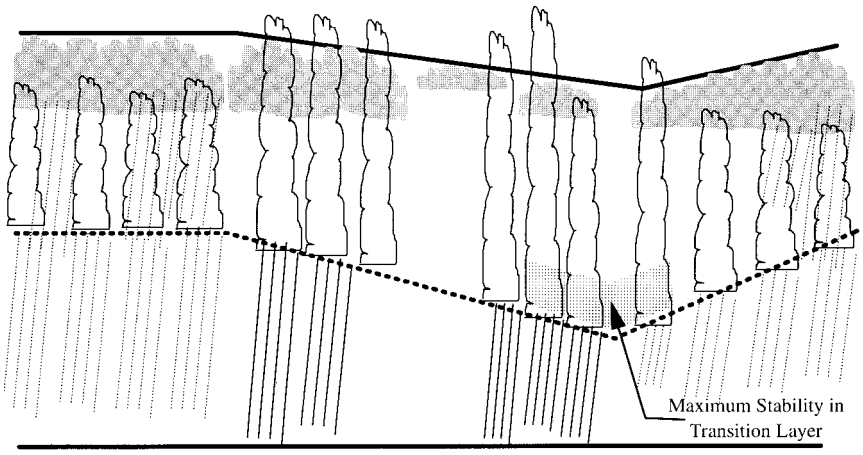

NIGHT	MORNING	AFTERNOON	EVENING
--thick, drizzling stratocumulus --shallow, weak cumulus --drizzle filling subcloud layer --lowest mean cloud thickness --highest mean cloud base --highest mean LCL	--drying of cloud layer --warming in stratus layer beneath the inversion --less numerous, increasingly vigorous cumulus --highest mean cloud thickness and lowest mean cloud base due to combination of thick stratocumulus and deep cumulus --measurable surface drizzle	--warming through most of the cloud layer --increasing stability in transition layer --accumulation of water vapor in the subcloud layer during late afternoon --increasing CAPE in the subcloud layer --deep, vigorous cumulus with mesoscale organization during late afternoon --largest surface drizzle rates of the day	--decreasing stability in the cloud layer --decreasing CAPE in the subcloud layer --more numerous, weak cumulus --thickening stratus --drizzle in subcloud layer, not reaching surface --detrainment of water vapor into the inversion layer --widest range of cloud base heights

FIG. 14. Schematic diagram of the diurnal cycle of cloud and boundary layer structure observed during the study period. The solid line at the bottom of the diagram is the ocean surface, the thick dotted line is the bottom of the transition layer (and LCL), and the thick solid line at the top of the diagram is z_i. Diagonal dotted and solid lines represent precipitation with the solid lines representing larger rainfall rates. Stratus are shaded with light gray and cumulus are not shaded. The time and location of the transition layer during the time of maximum stability is indicated.

convection. Conceptually, the increasing stability of the transition layer acts as a lid, creating a reservoir for water vapor and CAPE in the subcloud layer (Figs. 5–7). Because the transition layer is the most stable during this time, spontaneous convection is damped. In contrast, regions that exhibit mesoscale organization leading to convergence of subcloud water vapor may locally increase CAPE and lower the LCL. In these concentrated mesoscale regions, many cumulus may reach their level of free convection in spite of the high transition layer stability and may be quite energetic due to the amount of CAPE, producing relatively high updraft velocities and high surface drizzle rates. When the stability of the transition layer decreases at night, the likelihood of spontaneous convection increases, which prohibits substantial accumulations of water vapor and CAPE in the subcloud layer. Thus, the mechanism proposed by Rogers et al. may have a more pronounced influence on the cloud structure during the late afternoon and early evening, being predicated on the existence of mesoscale organization to provide the necessary CAPE to overcome the transition layer stability.

Liquid water structure was examined with a combination of cloud boundary measurements, integrated liquid water measurements, and theoretical calculations of the adiabatic integrated liquid water content from a parcel model. No pronounced diurnal signal in the liquid water structure was found (Fig. 12). Results showed that clouds thicker than approximately 450 m tended to have subadiabatic integrated liquid water contents (Figs. 12b and 12c), presumably due to evaporation of drizzle in the subcloud layer, removal of liquid water at the surface, and the evaporation of cloud water at cloud top. A significant fraction of clouds less than 450 m thick produced liquid water contents that were greater than adiabatic (Fig. 11) and there may be a physical mechanism that could produce such values in this cloud system (i.e., lateral detrainment of cloud water from con-

vective elements mixing with existing liquid water in decoupled stratus or with liquid water detrained by nearby convective elements). Unfortunately, instrument limitations may have also produced these greater-than-adiabatic values and the extent of instrument artifacts in these results is unclear. A study of the physical location and thermodynamic characteristics of the greater-than-adiabatic clouds showed them to be predominantly in the upper 400 m of the marine boundary layer and to be mostly decoupled. This finding, which is consistent with the physical mechanism outlined above, leads to the possibility that some of the observations are accurately portraying the liquid water stucture.

As a practical matter, the diurnal cycle yields important information about the relationships between the derivatives of the variables that drive cloud, precipitation, and thermodynamic structure. Since most cloud systems experience diurnal variability, one fruitful exercise that could lead to significant advances in global climate models is a concerted effort by the community to measure and simulate diurnal cycles. Such an effort is warranted because 1) simulating diurnal variability is a stringent test of model physics and 2) the necessary instrumentation to provide high quality observational data is currently available.

Acknowledgments. Dr. M. A. Miller was supported by the Brookhaven National Laboratory and by an appointment to the Global Change Distinguished Postdoctoral Fellowships, both sponsored by the U.S. Department of Energy. The latter appointment was administered by the Office of Health and Environmental Research through the Oak Ridge Institute for Science Education. Dr. E. E. Clothiaux's participation in ASTEX was supported by the Office of Health and Environmental Research through the Oak Ridge Institute for Science Education. Design and development of the 94-GHz radar was supported by the U.S. Navy Office of Naval Research (N00014-86-K-0688 and N00014-91-J-1991) and the U.S. Department of Energy (DE-FG02-90ER61071). We appreciate comments made by Dr. Bruce Albrecht, Dr. R. Michael Reynold, and Dr. Robert Pincus, as well as the efforts of Drs. Duynkereke and VilaGuerau de Arellano at the University of Utrecht in providing surface micrometeorological data. Dr. Xiquan Dong processed the radiometer data. We appreciated the comments of three reviewers and adopted many of their suggestions, including an expanded liquid water analysis. One of our reviewers suggested that afternoon convection in the transition region may be predicated on mesoscale organization, an excellent hypothesis. Mrs. Claire Lamberti provided invaluable editorial support.

This research was performed under the auspices of the United States Department of Energy under Contract DE-AC02-76CH00016.

APPENDIX A

The Conditional Sampling Criterion

As noted in the body of this paper, the conditional sampling criteria used in this study to filter unwanted island and synoptic effects is based on wind direction. Use of such a criterion presents a problem: what is the acceptable range of wind directions that minimizes island effects and represents the climatological synoptic flow in the region?

To arrive at an acceptable range of wind directions, the downstream effects of the larger island of San Miguel to the north must be considered. Linear back-trajectories imply that parcels arriving at the Santa Maria surface site have passed over San Miguel when the wind direction is between 325° and 4° (including 0°). The instruments used in this study were located on the northwestern coast of Santa Maria, so wind directions ranging from 70° to 200° (including 100°) suggest that the over-island fetch will be prohibitively large. Thus, a reasonable criterion would include 4° to 70° (including 40°) and ~200° to 325° (including 250°), although the latter of these ranges includes winds with a westerly component that is not consistent with climatology and must be excluded.

The synoptic-scale winds during ASTEX were determined using the 6-h analyses from the European Centre for Medium-Range Forecasts (ECMWF), which incorporated observations from ships in the region (Bretherton et al. 1995). In order to maximize the number of data points used in determination of the regional winds, the 10-m winds were averaged over a 1.25° by 1.25° latitude box with Santa Maria at its northwestern corner. This configuration was chosen because most of the supplemental soundings were made to the southeast of the island in the ASTEX experiment triangle.

The regional winds were supplemented by wind observations from independent platforms on Santa Maria because local effects could produce a substantial over-island fetch. It is assumed here that island-induced perturbations to the regional wind field will be larger during the daytime because the difference in surface temperature between the island and the surrounding ocean is the largest (Miller and Albrecht 1995). Furthermore, it is assumed that slightly longer fetches are acceptable during the night due to the high stability of the air over the island, which greatly reduces the depth of the internal boundary layer and prohibits interaction with the cloud layer above.

The 6-h regional ECMWF diagnosed winds were used as the first sampling criterion. If the regional wind direction was between 15° and 55° during the daytime or between 15° and 70° at night, the data were accepted as representative of the open ocean. Hourly winds from a sodar and micrometeorological system, each located within 200 m of the remote sensors, were used as the second level criterion. These hourly wind measurements are plotted in Fig. A1, along with the ECMWF 6-hourly,

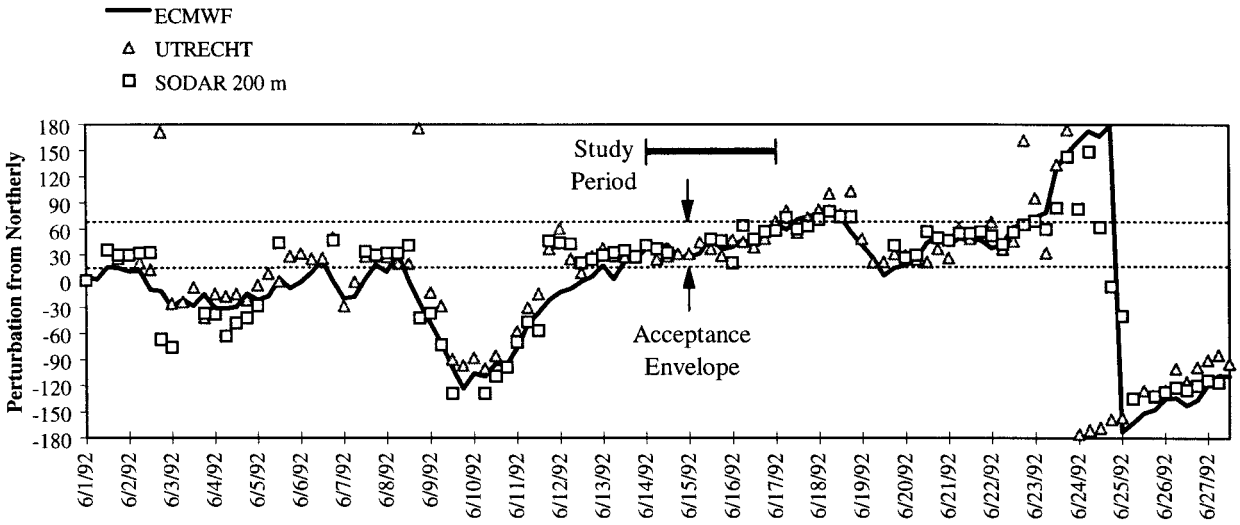

FIG. A1. Perturbation wind direction from 0° for Santa Maria during the ASTEX period from the ECMWF analysis, a surface micrometeorological system operated by the University of Utrecht, and from the 200-m observation gate of a nearby sodar system. The acceptance envelope for the conditional sampling criteria is indicated along with the study period.

10-m wind directions. The purpose of this exercise is to identify and exclude times during which the regional-scale winds are acceptable but the local winds are not. When the 200-m sodar winds were unavailable due to either equipment or signal-to-noise ratio problems, the 10-m winds from the micrometeorological tower were used as the sole criterion. This figure demonstrates the excellent agreement between the island-measured wind directions and those from the ECMWF analysis. The acceptance boundaries are indicated and the thick line indicates that the conditional sampling criterion was satisfied for the study period.

APPENDIX B

Calculation of the Integrated Adiabatic Liquid Water Content

Assuming parcels are undergoing adiabatic ascent from the measured cloud base to the measured cloud top, the integrated adiabatic liquid water content for each 30-s measurement of the cloud boundaries is computed using

$$\int_{\mathrm{CB}}^{\mathrm{CT}} d\chi = c_p \int_{\mathrm{CB}}^{\mathrm{CT}} \frac{(\Gamma_d - \Gamma_m)}{L}\, dz, \qquad \text{(B1)}$$

where χ is the liquid water content, CB denotes cloud base height, CT denotes cloud-top height, c_p is the specific heat at constant pressure, Γ_d is the dry adiabatic lapse rate (i.e., g/c_p, where g is gravity), Γ_m is the moist adiabatic lapse rate, L is the latent heat of condensation, and dz is a small increment in the height of the parcel. The moist adiabatic lapse rate is computed using

$$\Gamma_m = \Gamma_d \left(1 + \frac{Lw_s}{RT}\right)\left(1 + \frac{L^2 \varepsilon w_s}{Rc_p T^2}\right)^{-1}, \qquad \text{(B2)}$$

where T is the temperature, $R = 287.1$ J kg^{-1} K^{-1}, and $\varepsilon = 0.622$. Cloud base temperature is computed by assuming a dry adiabatic lapse rate in the subcloud layer, pressure is computed using the hydrostatic equation, and the total adiabatic liquid water content is determined by solving (B1) numerically for discrete layers.

REFERENCES

Albrecht, B. A., 1993: Effects of precipitation on the thermodynamic structure of the trade wind boundary layer. *J. Geophys. Res.*, **98,** 7327–7337.

——, C. W. Fairall, D. W. Thomson, and A. B. White, 1990: Surface-based remote sensing of the observed and the adiabatic liquid water content of stratocumulus clouds. *Geophys. Res. Lett.*, **17,** 89–92.

——, C. S. Bretherton, D. Johnson, W. H. Schubert, A. S. Frisch, 1995a: The Atlantic Stratocumulus Transition Experiment (ASTEX). *Bull. Amer. Meteor. Soc.*, **76,** 889–904.

——, M. P. Jensen, and W. J. Syrett, 1995b: Marine boundary layer structure and fractional cloudiness. *J. Geophys. Res.*, **100,** 14 209–14 221.

Betts, A. K., 1973: Non-precipitating cumulus convection and its parameterization. *Quart. J. Roy. Meteor. Soc.*, **99,** 178–196.

——, C. S. Bretherton, and E. Klinger, 1995: Relationship between mean boundary-layer structure and cloudiness at the R/V *Valdivia* during ASTEX. *J. Atmos. Sci.*, **52,** 2752–2762.

Bretherton, C. S., E. Klinker, A. K. Betts, and J. A. Coakley, 1995: Comparison of ceilometer, satellite, and synoptic measurements of boundary layer cloudiness and the ECMWF diagnostic cloud parameterization scheme during ASTEX. *J. Atmos. Sci.*, **52,** 2736–2751.

Clothiaux, E. E., M. A. Miller, B. A. Albrecht, T. A. Ackerman, J. Verlinde, D. M. Babb, R. M. Peters, and W. J. Syrett, 1995: An evaluation of a 94-GHz radar for remote sensing of cloud properties. *J. Atmos. Oceanic Technol.*, **12,** 201–229.

Harrison, E. F., P. Minnis, B. R. Barkstrom, V. Ramanathan, R. D. Cess, and G. G. Gibson, 1990: Seasonal variation of cloud radiative forcing derived from the Earth Radiation Budget Experiment. *J. Geophys. Res.*, **95,** 18 687–18 704.

Klein, S. A., D. L. Hartmann, and J. R. Norris, 1995: On the rela-

tionship among low cloud structure, sea surface temperature, and atmospheric circulation. *J. Climate*, **8,** 1140–1155.

Krueger, S. K., G. T. McLean, and Q. Fu, 1995: Numerical simulation of the stratus-to-cumulus transition in the subtropical marine boundary layer. Part I: Boundary layer structure. *J. Atmos. Sci.*, **52,** 2839–2850.

Lhermitte, R. M., 1987: A 94-GHz doppler radar for cloud observations. *J. Atmos. Oceanic Technol.,* **4,** 36–48.

Miller, M. A., and B. A. Albrecht, 1995: Surface-based observations of mesoscale cumulus-stratocumulus interaction during ASTEX. *J. Atmos. Sci.*, **52,** 2809–2826.

Nicholls, S., 1984: The dynamics of stratocumulus: Aircraft observations and comparisons with a mixed-layer model. *Quart. J. Roy. Meteor. Soc.*, **110,** 783–820.

Pincus, R., M. B. Baker, and C. S. Bretherton, 1997: What controls stratocumulus radiative properties? Lagrangian observations of cloud evolution. *J. Atmos. Sci.*, **54,** 2215–2235.

Ramanathan, V., R. D. Cess, E. F. Harrison, P. Minnis, B. R. Barkstrom, E. Ahmad, and D. Hartmann, 1989: Cloud-radiative forcing and climate: Results from the Earth Radiation Budget Experiment. *Science*, **243,** 57–63.

Randall, D. A., J. A. Coakley Jr., C. W. Fairall, R. A. Kropfli, and D. H. Lenschow, 1984: Outlook for research on subtropical marine stratiform clouds. *Bull. Amer. Meteor. Soc.*, **65,** 1290–1301.

Rogers, D. A., X. Yang, P. M. Norris, D. W. Johnson, G. M. Martin, C. A. Friehe, and B. W. Berger, 1995: Diurnal evolution of the cloud-topped marine boundary layer. Part I: Nocturnal stratocumulus development. *J. Atmos. Sci.,* **52,** 2953–2966.

Wang, S., 1993: Modeling marine boundary layer clouds with a two-layer model: A one-dimensional simulation. *J. Atmos. Sci.,* **50,** 4001–4021.

White, A. B., C. W. Fairall, and J. B. Snider, 1995: Surface-based remote sensing of marine boundary-layer cloud properties. *J. Atmos. Sci.*, **52,** 2827–2838.

Wyant, M. C., C. S. Bretherton, H. A. Rand, and D. A. Stevens, 1997: Numerical simulations and a conceptual model of the stratocumulus to trade cumulus transition. *J. Atmos. Sci.,* **54,** 168–192.